Journal of Power Sources 265 (2014) 125–131

Contents lists available at ScienceDirect

Journal of Power Sources

journal homepage: www.elsevier.com/locate/jpowsour

Performance of $Gd_{0.2}Ce_{0.8}O_{1.9}$ infiltrated $La_{0.2}Sr_{0.8}TiO_3$ nanofiber scaffolds as anodes for solid oxide fuel cells

Liquan Fan [a,b], Yueping Xiong [a,*], Lianbao Liu [a], Yuwei Wang [a,b], Haruo Kishimoto [c], Katsuhiko Yamaji [c], Teruhisa Horita [c]

[a] School of Chemical Engineering and Technology, Harbin Institute of Technology, 92 West Dazhi Street, Mailbox 1247, Harbin 150001, China
[b] College of Materials Science and Engineering, Qiqihar University, No. 42, Wenhua Street, Qiqihar 161006, China
[c] National Institute of Advanced Industrial Science and Technology (AIST), AIST Central No. 5, Higashi 1-1-1, Tsukuba, Ibaraki 305-8565, Japan

HIGHLIGHTS

- LST28 nanofibers were successfully synthesized by electrospinning method.
- LST28 nanofibers were sintered onto ScSZ electrolyte at 1000 °C for 2 h.
- LST28 nanofibers provide an efficient anchoring scaffold for the infiltrated GDC.
- LST28–GDC anode has a R_P value as low as 0.95 Ω cm^2 at 800 °C.
- LST28–GDC composite anodes show good thermal cycling stability.

GRAPHICAL ABSTRACT

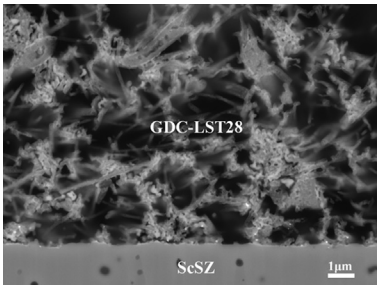

ARTICLE INFO

Article history:
Received 29 December 2013
Received in revised form
12 March 2014
Accepted 22 April 2014
Available online 9 May 2014

Keywords:
Solid oxide fuel cell
Composite anode
Gadolinia-doped ceria
Lanthanum strontium titanate
Nanofiber scaffold

ABSTRACT

LST28 nanofibers prepared by electrospinning can be sintered on ScSZ electrolyte at 1000 °C without formation of secondary phase. LST28 nanofibers with an electronic conduction pathway on ScSZ electrolyte provide an efficient anchoring scaffold for the infiltrated $Gd_{0.2}Ce_{0.8}O_{1.9}$ (GDC). The microstructure morphology and elemental distributions of $Gd_{0.2}Ce_{0.8}O_{1.9}$–$La_{0.2}Sr_{0.8}TiO_3$ (GDC–LST28) have been investigated in detail. GDC greatly improves the electrochemical performance of the fuel electrode. GDC–LST28 (0.92:1) composite anode gives the low interfacial polarization resistances (R_P) of 0.95, 0.63, 0.38 and 0.27 Ω cm^2 at 800, 850, 900 and 950 °C, respectively. The adding of GDC has greater influence on reducing low frequency region resistance of the polarization resistance than high frequency region resistance. The fuel cell with the GDC–LST28 composite anode has good thermal cycling stability.

1. Introduction

Nickel–yttria stabilized zirconia (Ni–YSZ) cermet is one of the most widely used anodes for solid oxide fuel cells (SOFCs). Ni plays a role as a fuel oxidation catalyst and electronic conductor; O^{2-} conducting YSZ inhibits the coarsening of Ni grains, keeps porous microstructure to enlarge triple-phase boundary (TPB), and makes the thermal expansion coefficient (TEC) of the anodes match with other component materials. The Ni-based cermet anode has many of the properties required for an efficient anode material. However, it has also some weaknesses for effective operation: those are carbon deposition for hydrocarbon fuels [1,2], sulfur poisoning and related nickel agglomeration [3–5], and redox unstability [6]. All these factors result in significant performance degradation of the

* Corresponding author. Tel.: +86 451 86413721; fax: +86 451 86418616.
E-mail address: ypxiong@hit.edu.cn (Y. Xiong).

http://dx.doi.org/10.1016/j.jpowsour.2014.04.109
0378-7753/

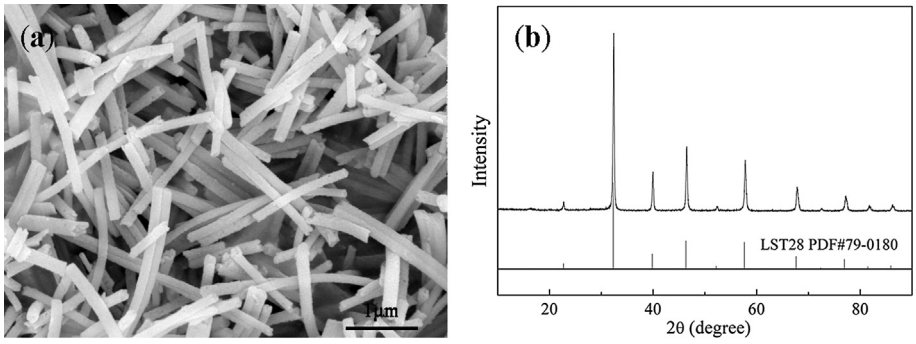

Fig. 1. SEM image (a) and XRD pattern (b) of LST28 nanofibers obtained by calcination of the as-electrospun precursor in air for 2 h at 900 °C. Standard X-ray diffraction peaks of LST28 (PDF#79-0180) are given as guides to the eyes at the bottom.

anodes and ultimately complete failure. So, researchers have been trying to develop other anode candidates to avoid these problems. The development of Ni-free anode with La doped $SrTiO_3$ (LST) has received increasing attention due to their tolerance for sulfur poisoning and carbon deposition [7]. In 1997, John T.S. Irvine first used A-site deficient perovskite $Sr_{1-3x/2}La_xTiO_{3-\delta}$ ($0 \leq x \leq 0.6$) as potential anode materials for SOFCs [8]. And then $La_xSr_{1-x}TiO_3$ ($x = 0.1$, 0.2, 0.3, 0.35, and 0.4) was found to have good dimensional and chemical stability when subjected to redox cycling, and the TEC of $La_xSr_{1-x}TiO_3$ was comparable with that of YSZ [9]. LST possesses high electronic conductivity but very low ionic conductivity in reducing atmospheres [8,10]. Yashiro [11] reported that $La_{0.2}Sr_{0.8}TiO_3$ (LST28) anode gives the polarization resistance of 350 Ω cm^2 at 800 °C using H_2 as fuel gas. As mentioned above, single LST is not suitable to be used as anode for SOFCs because of its low catalytic activity for electrochemical oxidation process. Many of doped and undoped ceria [12–16] have been added into LST phase to form composite anodes with good electrochemical performance. The presence of cerium-rich phase in composite electrodes can greatly enhance the electrocatalytic activity for hydrogen oxidation [17,18]. In addition, many studies have discovered that both ceria and doped ceria are potential SOFC anode materials [19–21]. An area specific polarization resistance of $Ce_{0.6}Gd_{0.4}O_{1.8}$ anode gives 0.39 Ω cm^2 at 1000 °C in $H_2/H_2O/N_2 = 9/1.2/89.8$ fuel gas [19].

In the present work, we applied electrospinning technique to synthesize LST28 nanofibers, and designed and synthesized $Gd_{0.2}Ce_{0.8}O_{1.9}$–$La_{0.2}Sr_{0.8}TiO_3$ (GDC–LST28) composite anodes using LST28 nanofiber scaffolds with the infiltrated GDC. The robustness of LST28 nanofibers makes them suitable as a conducting scaffold and the absence of catalytic activity and O^{2-} conduction can be compensated by infiltration with GDC. The microstructure of the GDC–LST28 composite anode and the effect of the infiltrated GDC on the enhancement of electrochemical performance of the fuel electrode were investigated in detail.

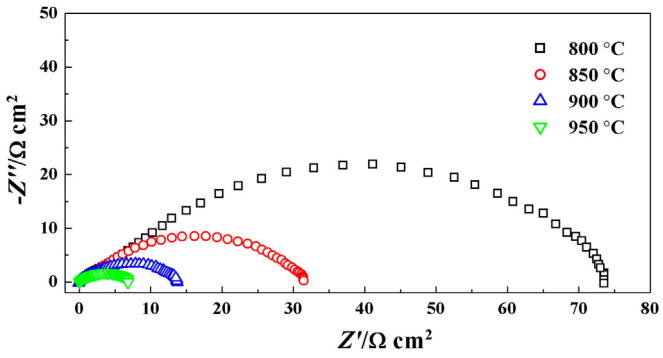

Fig. 2. Impedance spectra of the LST28 anode measured at 800, 850, 900 and 950 °C with 97% H_2 + 3% H_2O as fuel gas.

2. Experimental method

2.1. Preparation

2.1.1. Preparation of LST28 nanofibers

Appropriate amounts of polyvinylpyrrolidone (PVP) and concentrated nitric acid were dissolved into *N*,*N*-dimethylformamide (DMF) at room temperature under stirring until the solution became clear. And then stoichiometric amounts of $La(NO_3)_3 \cdot 6H_2O$, $Sr(NO_3)_2$ and $Ti(OC_3H_7)_4$ with molar ratios of 0.2:0.8:1 were added into the above acidic solution to get a homogeneous precursor solution of 8 wt.% PVP and 18 wt.% metal salts for electrospinning. The precursor solution was loaded into a plastic syringe equipped with a flat stainless steel needle of 0.8 mm in diameter. A high voltage supply was connected to the spinneret (stainless steel needle) and a nickel mesh collector was placed 12 cm away from the orifice. The electric voltage was set at 22 kV. The as-electrospun

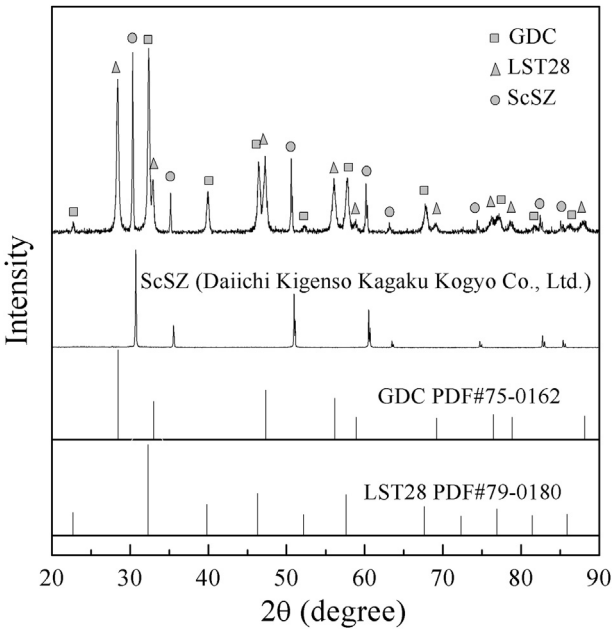

Fig. 3. XRD pattern of GDC–LST28 composite anode in 0.84:1 mass ratio of GDC to LST28 on ScSZ electrolyte. Standard X-ray diffraction peaks of LST28 (PDF#79-0180), GDC (PDF#75-0162) and the measured XRD pattern of ScSZ (Daiichi Kigenso Kagaku Kogyo Co., Ltd.) are given as guides to the eyes at the bottom.

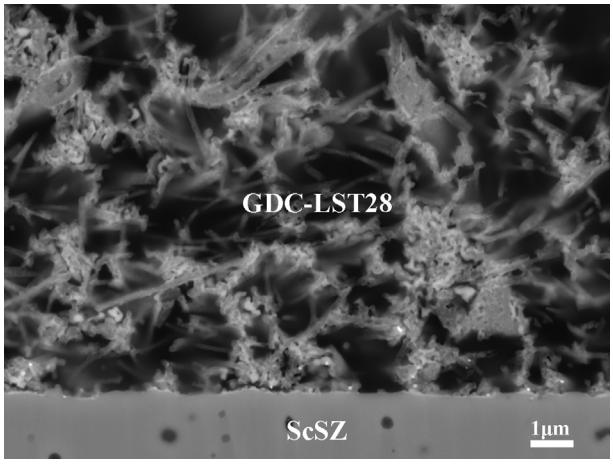

Fig. 4. Cross-section SEM micrograph of GDC–LST28 (0.84:1) composite anode on ScSZ electrolyte.

precursor nanofibers were calcined in air at 900 °C for 2 h, and then crumbed into short rod-like LST28 nanofibers.

2.1.2. Preparations of GDC–LST28 composite anodes and single cells

$Ce(NO_3)_3 \cdot 6H_2O$ and $Gd(NO_3)_3 \cdot 6H_2O$ in a mole ratio of 0.2:0.8 were dissolved into a mixture solution of ethyl alcohol and deionized water (50:50 vol.%), followed by the addition of glycine as complexing agent. The mole ratio of metal cations to glycine was 2:1, eventually forming a precursor solution of GDC containing 0.25 mol L^{-1} metal cations for infiltration.

Platinum paste was coated in diameter of 10 mm onto one side of 1 mol% CeO_2–10 mol% Sc_2O_3–89 mol% ZrO_2 (ScSZ, Daiichi Kigenso Kagaku Kogyo Co., Ltd.) electrolyte disks with a diameter of about 19 mm and a thickness of 0.5 mm–0.6 mm, and fired at 1000 °C for 1 h to serve as the cathode. The effective cathode area was 0.785 cm^2. Pt reference electrode was prepared on the rim of the ScSZ disk. The LST28 nanofibers were mixed with 3 wt.%-ethyl cellulose terpineol solution in 1:1 mass ratio to be made into slurry. Then the slurry was coated on the opposite side of the ScSZ electrolyte disk to the cathode symmetrically and subsequently sintered at 1000 °C for 2 h, forming a LST28 nanofiber scaffold with a diameter of 10 mm and a thickness of about 50 μm on the ScSZ electrolyte. The mass was measured for several LST28 nanofiber scaffold samples and the average value was about 2.5 mg, and the apparent area of the circular scaffold electrode was 0.785 cm^2. GDC-LST28 composite anodes with different mass ratios of GDC to LST28 were fabricated by infiltrating different amount of GDC precursor solution into LST28 nanofiber scaffolds and sintering at 800 °C for 1 h. Pt cathode, ScSZ electrolyte and LST28 anode (or GDC–LST28 composite anode) constituted a SOFC single cell. Pt mesh and Au mesh were used as current collector for the cathode and the anode, respectively.

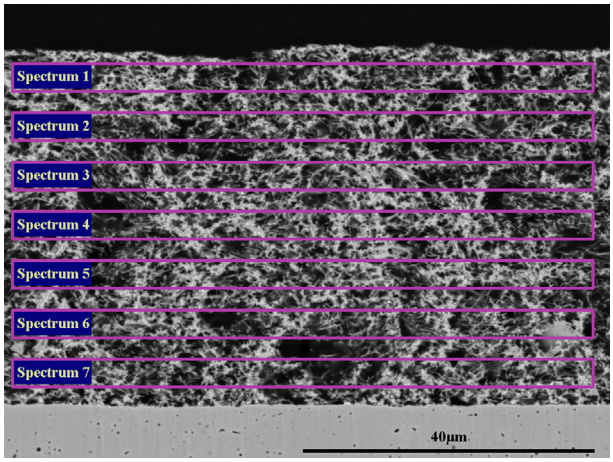

Fig. 5. Cross-section SEM image of GDC–LST28 (0.84:1) composite anode on ScSZ electrolyte used for elemental area analysis of atom concentration (%).

Table 1
Elemental area analysis of atom concentration (%) for GDC–LST28 (0.84:1) composite anode.

Spectrum	Statistics	O	Ti	Sr	La	Ce	Gd
Spectrum 1	Yes	70.20	10.29	9.98	2.35	6.05	1.13
Spectrum 2	Yes	70.40	10.51	9.91	2.23	5.48	1.46
Spectrum 3	Yes	69.81	10.71	9.84	2.24	5.95	1.45
Spectrum 4	Yes	68.68	10.66	10.00	2.33	6.61	1.72
Spectrum 5	Yes	68.93	10.81	9.76	2.08	6.78	1.65
Spectrum 6	Yes	68.60	11.30	11.05	1.91	5.70	1.44
Spectrum 7	Yes	66.58	11.93	10.87	2.60	6.39	1.63
Average		69.03	10.89	10.20	2.25	6.14	1.50
Standard deviation		1.30	0.55	0.53	0.22	0.48	0.20
Maximum		70.40	11.93	11.05	2.60	6.78	1.72
Minimum		66.58	10.29	9.76	1.91	5.48	1.13

2.2. Characterization and test

The metal composition of LST28 nanofibers obtained through calcination of as-electrospun precursor nanofibers at 900 °C was determined by inductively coupled plasma atomic emission spectroscopy (ICP-AES) with an Optima 5300DV spectrometer. The microstructure and phase formation of LST28 were examined by scanning electron microscopy (SEM, FEI Quanta 200, Netherlands) and X-ray diffraction (XRD, Rigaku D/max-IIB) using Cu-Kα radiation, respectively. Phases in the GDC–LST28 composite anode on ScSZ electrolyte were identified by XRD. Cross-sectional microstructure and elemental distribution of the GDC–LST28 composite anode were characterized by a Field Emission Scanning Electron Microscope (FE-SEM, JSM-7001F, JEOL) equipped with Energy Dispersive Spectrometer (EDS, OXFORD INSTRUMENTS). The surface morphology and elemental distribution of a single GDC-infiltrated LST28 nanofiber were analyzed by transmission electron microscopy (FEI Tecnai-F20 TEM) and EDS elemental mapping in TEM. Carbon-coated copper grids were used as the sample holders.

The single cells consisting of Pt cathode, ScSZ electrolyte and LST28 anode (or GDC–LST28 composite anode) were used for electrochemical tests in the temperature range of 800–1000 °C. The cathode was exposed to air atmosphere while the anode was fed with 97% H_2 + 3% H_2O fuel gas. Polarization resistances of the anodes, the *I–V* and *I–P* characteristics and thermal cycling performance of the single cells were measured using an electrochemical workstation (CS310, CorrTest, China).

3. Results and discussion

The ICP analysis result of the LST28 nanofibers obtained by the electrospinning method show that the elemental proportions of La, Sr and Ti are 0.203, 0.795 and 1.00, respectively. So, we can confirm that the actual composition of the sample is consistent with the expected nominal composition of $La_{0.2}Sr_{0.8}TiO_3$.

Fig. 1(a) shows the SEM image of the LST28 nanofibers obtained by calcination of the as-electrospun precursor in air for 2 h at 900 °C. The nanofibers show smooth surface and relatively uniform

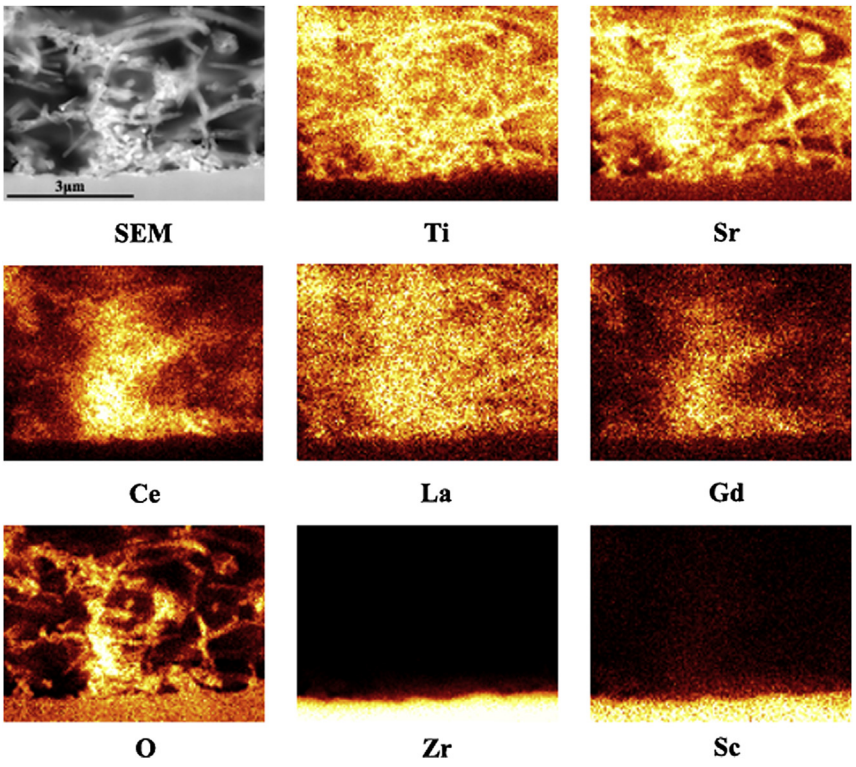

Fig. 6. Cross-section SEM image and elemental distributions of GDC–LST28 (0.84:1) composite anode on ScSZ electrolyte.

length. The diameter is about 200 nm. The XRD pattern of the LST28 nanofibers is shown in Fig. 1(b). For comparison, the standard diffraction peaks of LST28 (PDF#79-0180) are displayed at the bottom of Fig. 1(b). All the observed diffraction peaks were identified as single phase of LST28 with cubic perovskite structure. The LST nanofibers can be obtained with very low calcination temperature of 900 °C and short process time of 2 h. The adopted electrospinning technique provides an effective step towards preparing phase pure $La_{0.2}Sr_{0.8}TiO_3$ (LST28) formed at lower temperature compared to the sintering temperature adopted in other methods such as glycine/nitrate combustion synthesis [9], solid-state reaction method [22–25] and Pechini method [26] and so on, which facilitates the implementation of low electrode–electrolyte sintering temperature.

In order to avoid the formation of secondary phase at 1200 °C in firing process [25], the LST28 nanofiber slurry was sintered onto ScSZ electrolyte at 1000 °C for 2 h. To verify the possibility of LST28 serving alone as anode, the polarization resistances (R_P) of the LST anode were measured in the temperature range of 800–950 °C, as shown in Fig. 2. The anode shows high R_P values. It is indicative that single phase LST28 nanofiber is not suitable to be used as anode alone.

We infiltrated GDC precursor into LST28 nanofiber scaffold to form GDC–LST28 composite anodes. Fig. 3 shows the XRD pattern of GDC-LST28 composite anode in 0.84:1 mass ratio of GDC to LST28 (hereafter referred to simply as GDC–LST28 (0.84:1)) on ScSZ electrolyte. The standard diffraction X-ray peaks of LST28 (PDF#79-0180), GDC (PDF#75-0162) and the measured XRD pattern of ScSZ (Daiichi Kigenso Kagaku Kogyo Co., Ltd.) are also given as guides to the eyes at the bottom of Fig. 3. All the diffraction peaks were indexed to LST28, GDC and ScSZ. There were no clearly detectable peaks from secondary phase. A cross-section SEM micrograph of GDC–LST28 (0.84:1) composite anode on ScSZ electrolyte is presented in Fig. 4. The sintered LST28 nanofibers on ScSZ electrolyte are randomly oriented and there are many junction points between the fibers, forming a three-dimensional scaffold to effectively anchor the infiltrated GDC nanoparticles and provide sufficient adhesion between anode and electrolyte. At the same time, the LST28 nanofiber scaffold possesses a porous structure which facilitates fluent gas transport. A cross-section SEM image of GDC–LST28 (0.84:1) composite anode on ScSZ electrolyte used for elemental area analysis of atom concentration (%) is shown in Fig. 5. The elemental area analysis results of atom concentration (%) are summarized in Table 1. The uniform distributions of Gd and Ce show that the infiltrated GDC is evenly spread throughout the whole LST28 nanofiber scaffold. Fig. 6 shows elemental distribution maps for GDC–LST28 (0.84:1) composite anode with ScSZ electrolyte. The distributions of La, Sr and Ti element show clear contour profiles of the LST28 nanofibers' distribution throughout the composite anode. The LST28 nanofibers are randomly-ordered and there are many junction points between the LST28 nanofibers, which were established through conjugation during the calcination of the LST28 slurry, therefore, the LST28 nanofiber scaffold builds an electronic conduction path in three dimensions. While Gd and Ce appear almost exactly where there're La, Sr and Ti. Fig. 7 shows the TEM image of GDC–LST28 (0.84:1) composite and the corresponding EDS elemental mapping. The distributions of Gd and Ce proof that GDC is dispersed on the surface of LST28 nanofibers rather uniformly, which further affirms the efficient anchoring role of LST28 nanofiber scaffold. These GDC nanoparticles attached to LST28 nanofibers form a mixed ionic-electronic conducting path. All of the above-mentioned factors can result in the enlargement of TPB for electrochemical reaction.

The mass ratio of GDC to LST28 was varied to optimize the R_P values for the composite anodes. The impedance spectra and fitting results for GDC–LST28 (0.92:1) measured at 800, 850, 900 and 950 °C in 97% H_2 + 3% H_2O atmosphere are shown in Fig. 8. Impedance spectrum appeared as two depressed capacitive arcs,

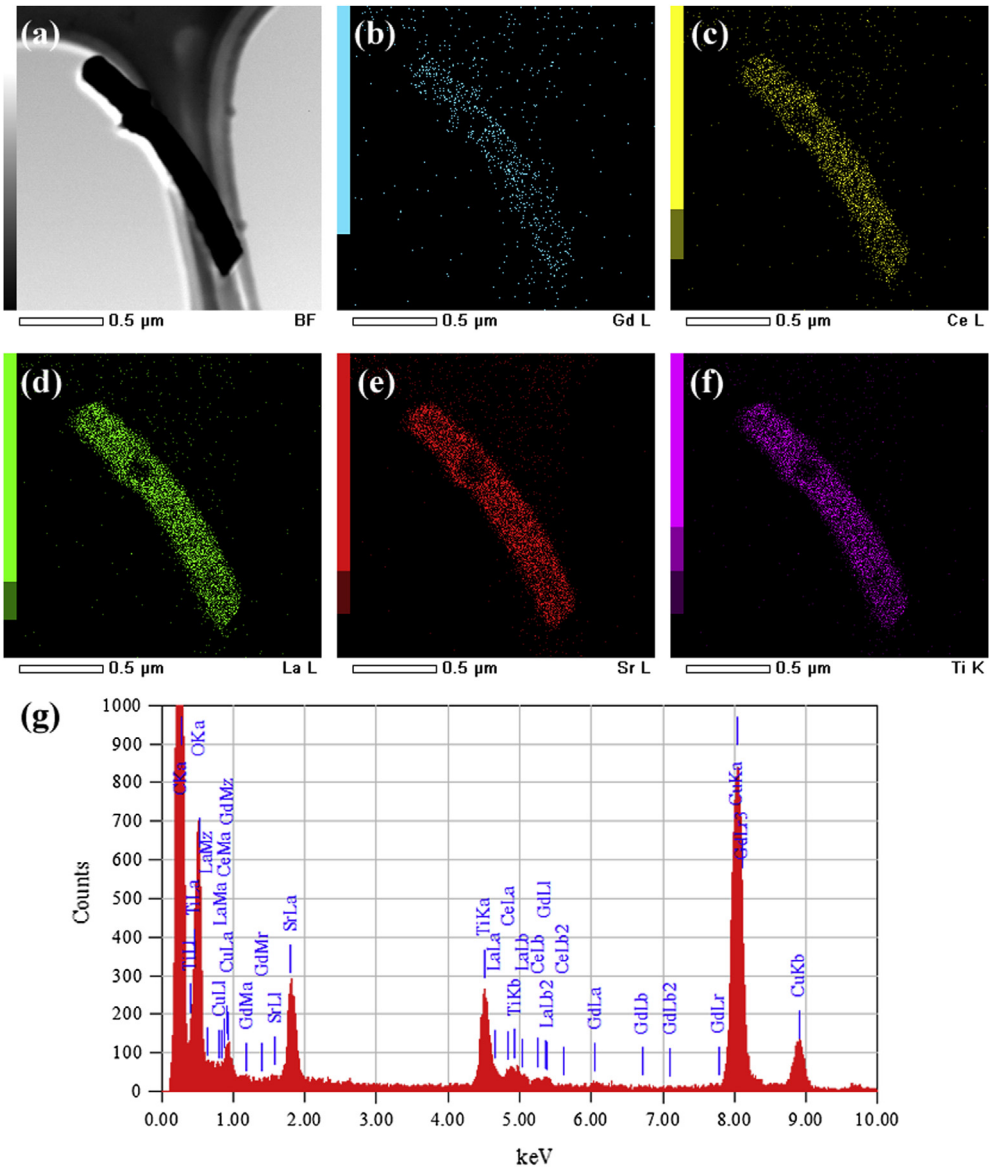

Fig. 7. (a) TEM image of GDC-LST28 (0.84:1) composite, the corresponding EDS elemental mapping: (b) Gd, (c) Ce, (d) La, (e) Sr, and (f) Ti, and (g) EDS.

which can be fitted by the equivalent circuit also shown in Fig. 8. Here L is an inductance and Q a constant phase element. The resistances of R_1, R_2 and R_3 represent ohmic resistance, high frequency region resistance and low frequency region resistance, respectively. R_2 and R_3 constitute R_P. According to the analysis in literature [27–29], the impedance in high frequency region is attributed to charge transfer process occurring at the interfaces, while that in low frequency region is normally ascribed to the surface adsorption/desorption, surface diffusion, and surface reaction processes of hydrogen species. The interfacial polarization resistance and its components in different frequency regions in different frequency regions as a function of various GDC:LST28 mass ratio are shown in Fig. 9. As shown in Fig. 9(a), the R_P values decreased with the increasing amount of infiltrated GDC up to the 0.92:1 mass ratio, after which no change was observed until GDC:LST28 ratio of 1.31:1. Then, we applied the fitting results of the equivalent circuit to find the general tendency of the variation of R_2 and R_3 with the GDC loading level. By comparing Fig. 9(b) with (c), the adding of GDC has greater influence on reducing low frequency

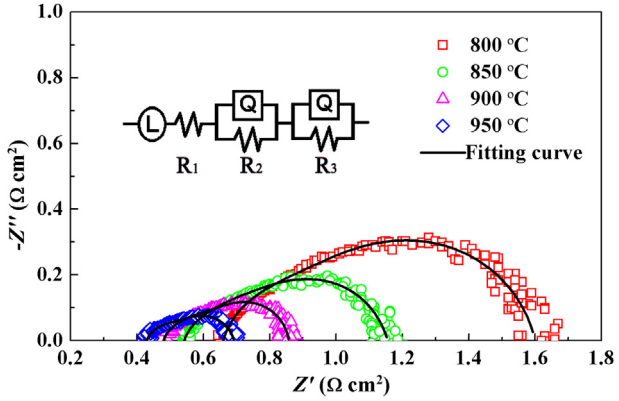

Fig. 8. Impedance spectra and fitting results of GDC–LST28 (0.92:1) composite anode in 97% H_2 + 3% H_2O atmosphere at 800, 850, 900 and 950 °C and the corresponding equivalent circuit.

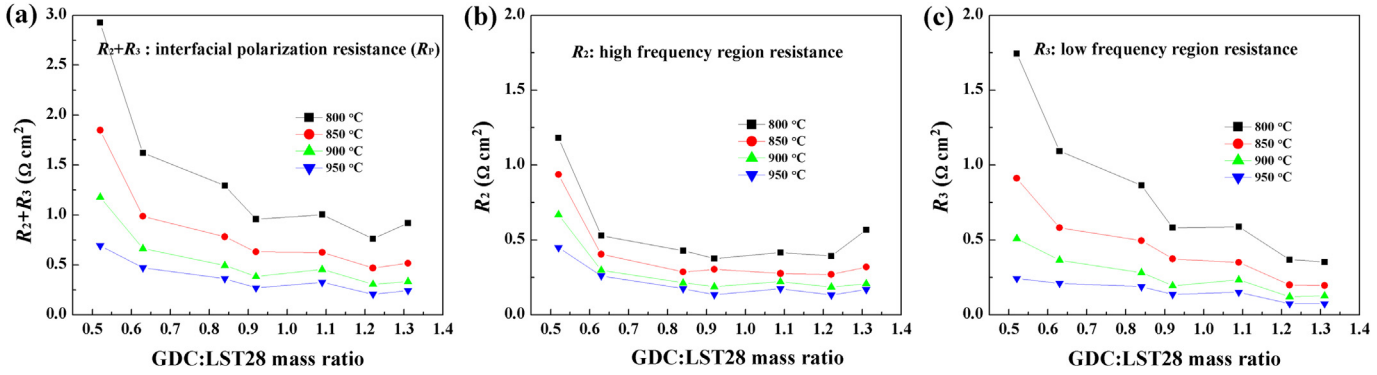

Fig. 9. Variation in the resistance values of (a) $R_2 + R_3$, (b) R_2 and (c) R_3 as a function of the GDC:LST28 mass ratio at measurement temperature of 800, 850, 900 and 950 °C for the GDC–LST28 composite anodes.

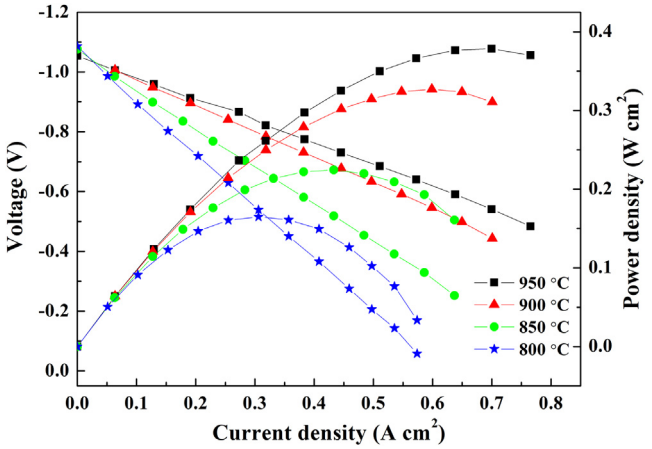

Fig. 10. *I–V* and *I–P* curves for the single cell consisting of GDC–LST28 (0.92:1) composite anode, ScSZ electrolyte and Pt cathode tested at 800 °C, 850 °C, 900 °C and 950 °C. 97% H_2 + 3% H_2O was on the anode side and air was on the cathode side.

region resistance (R_3) of R_P than high frequency region resistance (R_2). This is consistent with the result reported in literature [21].

It can be seen from the impedance spectra in Fig. 8(d) that GDC–LST28 (0.92:1) shows the lowest R_P and the R_P values were 0.95, 0.63, 0.38 and 0.27 Ω cm^2 at 800, 850, 900 and 950 °C, respectively. At 800 °C, the R_P value of 0.95 Ω cm^2 was lower than the result (2.1 Ω cm^2) in literature reported by Yoo et al. [14]. The single cell performance with the GDC–LST28 (0.92:1) composite anode at different temperatures is shown in Fig. 10. The cell showed an OCV of approximately 1.06 V and a power density of 0.38 W cm^2 at 950 °C. The OCV value is close to the theoretical one. The obtained power density was not very high due to the thick ScSZ electrolyte mainly accounting for the total resistance of the cell, as a large electrolyte ohmic resistance can be seen from Fig. 8. The relatively high cell performance is expected by making the thickness of the electrolyte very thin or using higher ionic conducting electrolyte such as lanthanum strontium gallium magnesium oxides (LSGM) [30] and these studies are underway.

To study the stability of GDC–LST28, a thermal cycling test of the single cell with GDC–LST28 (0.88:1) composite anode was conducted according to the temperature profiles as shown in Fig. 11(a). A cycle comprised 4 stages: heating, holding at 950 °C, cooling, and holding at 550 °C for 30 min respectively. The cell worked at a constant voltage of 0.557 V. Simultaneously, the corresponding current density was recorded during the cycling duration, as shown in Fig. 11(b). After 3120-min 26 cycles, the single cell exhibited no performance degradation, which demonstrated a good thermal cycling stability of the GDC–LST28 composite anode.

4. Conclusions

LST28 nanofibers were successfully sintered onto ScSZ electrolyte at 1000 °C without the formation of secondary phase, which provide an efficient anchoring scaffold for the infiltrated GDC. The electrochemical performance of anodes was greatly enhanced by the presence of GDC which has greater influence on reducing low frequency region resistance (R_3) of R_P than high frequency region resistance (R_2). The GDC–LST28 (0.92:1) composite anode gives the

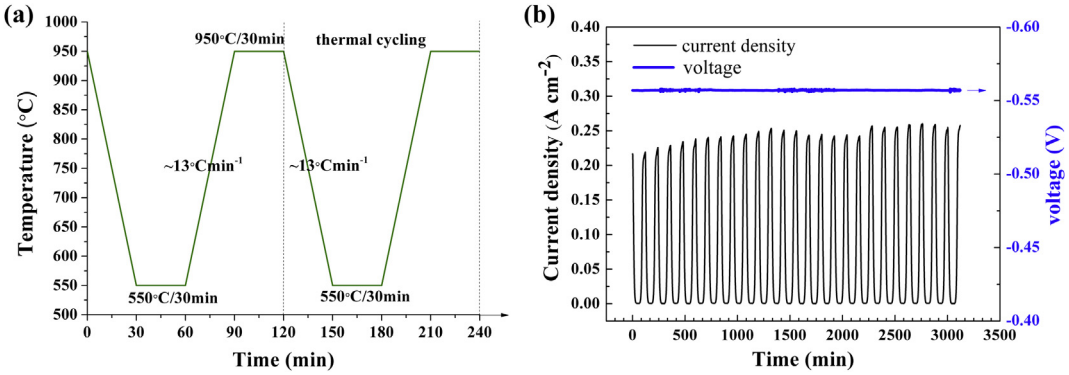

Fig. 11. (a) Temperature profile for thermal cycling, (b) the corresponding time dependence of current density at 0.557 V for the single cell with GDC–LST28 (0.88:1) composite anode.

interfacial polarization resistances of 0.95, 0.63, 0.38 and 0.27 Ω cm^2 at 800, 850, 900 and 950 °C, respectively. The GDC–LST28 composite anode has good thermal cycling stability.

Acknowledgments

This work was supported by the National Natural Science Foundation of China (51072040) and the National Program on Key Basic Research Project (973 Program 2012CB215400).

References

[1] T. Takeguchi, Y. Kani, T. Yano, R. Kikuchi, K. Eguchi, K. Tsujimoto, Y. Uchida, A. Ueno, K. Omoshiki, M. Aizawa, J. Power Sources 112 (2002) 588–595.
[2] M. Yoshinaga, H. Kishimoto, K. Yamaji, Y.P. Xiong, M.E. Brito, T. Horita, H. Yokokawa, Solid State Ionics 192 (2011) 571–575.
[3] Y. Matsuzaki, I. Yasuda, Solid State Ionics 132 (2000) 261–269.
[4] H. Kishimoto, K. Yamaji, T. Horita, Y.P. Xiong, N. Sakai, M.E. Brito, H. Yokokawa, J. Power Sources 172 (2007) 67–71.
[5] H. Kishimoto, Y.P. Xiong, K. Yamaji, T. Horita, N. Sakai, M.E. Brito, H. Yokokawa, J. Chem. Eng. Jpn. 40 (2007) 1178–1182.
[6] B. Iwanschitz, J. Sfeir, A. Mai, M. Schutze, J. Electrochem. Soc. 157 (2010) B269–B278.
[7] X.M. Ge, S.H. Chan, Q.L. Liu, Q. Sun, Adv. Energy Mater. 2 (2012) 1156–1181.
[8] P.R. Slater, D.P. Fagg, J.T.S. Irvine, J. Mater. Chem. 7 (1997) 2495–2498.
[9] O.A. Marina, N.L. Canfield, J.W. Stevenson, Solid State Ionics 149 (2002) 21–28.
[10] R. Moos, S. Schöllhammer, K.H. Härdtl, Appl. Phys. A: Mater. Sci. Process 65 (1997) 291–294.
[11] K. Yashiro, T. Kobayashi, L.Q. Han, A. Kaimai, Y. Nigara, T. Kawada, J. Mizusaki, K. Kawamura, in: H. Yokokawa, S.C. Singhal (Eds.), Solid Oxide Fuel Cells VII (SOFC VII), Electrochemical Society, Pennington, 2001, pp. 678–683.
[12] X.F. Sun, S.R. Wang, Z.R. Wang, X.F. Ye, T.L. Wen, F.Q. Huang, J. Power Sources 183 (2008) 114–117.
[13] K.B. Yoo, G.M. Choi, Solid State Ionics 180 (2009) 867–871.
[14] K.B. Yoo, G.M. Choi, Solid State Ionics 192 (2011) 515–518.
[15] C.D. Savaniu, J.T.S. Irvine, Solid State Ionics 192 (2011) 491–493.
[16] M. Roushanafshar, J.L. Luo, A.L. Vincent, K.T. Chuang, A.R. Sanger, Int. J. Hydrogen Energy 37 (2012) 7762–7770.
[17] O.A. Marina, L.R. Pederson, in: Proceedings of the 5th European Solid Oxide Fuel Cells Forum, 2002, pp. 481–489.
[18] H. Kishimoto, K. Yamaji, Y.P. Xiong, T. Horita, N. Sakai, M.E. Brito, H. Yokokawa, IEEJ Trans. Fundam. Mater. 128 (2008) 333–338.
[19] O.A. Marina, C. Bagger, S. Primdahl, M. Mogensen, Solid State Ionics 123 (1999) 199–208.
[20] M. Mogensen, T. Lindegaard, U.R. Hansen, G. Mogensen, J. Electrochem. Soc. 141 (1994) 2122–2128.
[21] T. Nakamura, K. Yashiro, A. Kaimai, T. Otake, K. Sato, T. Kawada, J. Mizusaki, J. Electrochem. Soc. 155 (2008) B1244–B1250.
[22] Y. Gan, Q.Q. Qin, S.G. Chen, Y. Wang, D.H. Dong, K. Xie, Y.C. Wu, J. Power Sources 245 (2014) 245–255.
[23] D. Neagu, J.T.S. Irvine, Chem. Mater. 22 (2010) 5042–5053.
[24] J.C. Ruiz-Morales, J. Canales-Vazquez, C. Savaniu, D. Marrero-Lopez, W.Z. Zhou, J.T.S. Irvine, Nature 439 (2006) 568–571.
[25] G. Chen, H. Kishimoto, K. Yamaji, K. Kuramoto, T. Hortia, in: The 21th Symposium on Solid Oxide Fuel Cells in Japan, 2012, pp. 92–95.
[26] B.K. Park, J.W. Lee, S.B. Lee, T.H. Lim, S.J. Park, R.H. Song, W.B. Im, D.R. Shin, Int. J. Hydrogen Energy 37 (2012) 4319–4327.
[27] A. Torabi, T.H. Etsell, J. Power Sources 225 (2013) 51–59.
[28] Q.A. Huang, R. Hui, B.W. Wang, J.J. Zhang, Electrochim. Acta 52 (2007) 8144–8164.
[29] S. Primdahl, M. Mogensen, J. Electrochem. Soc. 144 (1997) 3409–3418.
[30] K.Q. Huang, R. Tichy, J.B. Goodenough, C. Milliken, J. Am. Ceram. Soc. 81 (1998) 2581–2585.